Radar Signatures Associated with Quasi-Linear Convective System Mesovortices

CHARLES M. KUSTER,[a] KEITH D. SHERBURN,[d] VIVEK N. MAHALE,[e] TERRY J. SCHUUR,[a,b,c] OLIVIA F. MCCAULEY,[f] AND JASON S. SCHAUMANN[g]

[a] *NOAA/OAR National Severe Storms Laboratory, Norman, Oklahoma*
[b] *Cooperative Institute for Severe and High Impact Weather Research and Operations, Norman, Oklahoma*
[c] *School of Meteorology, University of Oklahoma, Norman, Oklahoma*
[d] *NOAA/National Weather Service, Rapid City, South Dakota*
[e] *NOAA/National Weather Service, Norman, Oklahoma*
[f] *Iowa State University, Ames, Iowa*
[g] *NOAA/National Weather Service, Springfield, Missouri*

(Manuscript received 16 August 2023, in final form 14 May 2024, accepted 11 June 2024)

ABSTRACT: Recent operationally driven research has generated a framework, known as the three ingredients method and mesovortex warning system, that can help forecasters anticipate mesovortex development and issue warnings within quasi-linear convective systems (QLCSs). However, dual-polarization radar data has not yet been incorporated into this framework. Therefore, several dual- and single-polarization radar signatures associated with QLCS mesovortices were analyzed to determine if they could provide additional information about mesovortex development and intensity. An analysis of 167 mesovortices showed that 1) K_{DP} drops precede ~95% of mesovortices and provide an initial indication of where a mesovortex may develop; 2) midlevel K_{DP} cores are a potentially useful precursor signature because they precede a majority of mesovortices and have higher magnitudes for mesovortices that produce wind damage or tornadoes; 3) low-level K_{DP} cores and areas of enhanced spectrum width have higher magnitudes for mesovortices that produce wind damage or tornadoes but tend to develop at about the same time as the mesovortex, which makes them more useful as diagnostic than as predictive signatures; and 4) as range from the radar increases, the radar signatures become less useful in anticipating mesovortex intensity but can still be used to anticipate mesovortex development or build confidence in mesovortex existence.

SIGNIFICANCE STATEMENT: The purpose of this study is to look at weather radar features that might help forecasters predict the development and intensity of tornadoes and strong winds within linear thunderstorm systems. Our results show that the intensity and trends of some radar features are helpful in showing when these hazards might develop and how strong they might be, while other radar features are less helpful. This information can help forecasters focus on the most useful radar features and ultimately provide the best possible warnings.

KEYWORDS: Convective storms; Mesoscale processes; Radars/Radar observations; Nowcasting

1. Introduction

Quasi-linear convective systems (QLCSs) are responsible for about 21% of all tornado reports and 28% of all severe wind reports across the United States, and these percentages are even higher across the southeastern United States, especially during the cool season (Ashley et al. 2019). Due to this high prevalence of reports, scientists are currently working to understand more about QLCSs through numerical simulations, observations, and field projects (e.g., Atkins and St. Laurent 2009; Davis and Parker 2014; Marion and Trapp 2021; Goodnight et al. 2022). Mesovortices, which are storm-scale, low-level circulations that can be associated with damaging winds, tornadoes, or both (e.g., Przybylinski 1995; Weisman and Trapp 2003; Atkins et al. 2004), are an important aspect of QLCSs. To increase mesovortex predictability, research led by forecasters within the National Weather Service (NWS) developed the three ingredients method (Schaumann and Przybylinski 2012; Gibbs 2021), which combines environmental and radar information to help forecasters anticipate the development of mesovortices. Building on this research, recent work done within the NWS Central Region Convective Warning Improvement Project added 14 radar-based and environmentally based factors, known as confidence builders and nudgers, to the three ingredients method to create the mesovortex warning system (NWS 2023, summary at https://www.weather.gov/media/sgf/research/TWIP_QLCS_Reference_Sheets.pdf). One goal of the mesovortex warning system is to provide forecasters with guidance on whether a severe thunderstorm or tornado warning is best suited for an anticipated or ongoing mesovortex. While some questions remain regarding how best to determine environmental vertical wind shear values for the mesovortex warning system (e.g., Ungar and Coniglio 2023), Gibbs (2021) found that applying the mesovortex warning system was skillful in anticipating

Supplemental information related to this paper is available at the Journals Online website: https://doi.org/10.1175/WAF-D-23-0144.s1.

Corresponding author: Charles M. Kuster, charles.kuster@noaa.gov

DOI: 10.1175/WAF-D-23-0144.1

mesovortex development and provided a starting point for a tornado warning decision threshold. As a result, elements of the mesovortex warning system have been incorporated into existing training provided by the Warning Decision Training Division (WDTD 2020).

Despite recent progress in understanding and predicting QLCS tornadoes, they remain a significant forecast challenge. Currently, tornado warnings issued for QLCS tornadoes have a lower probability of detection when compared to supercell tornado warnings and what might be expected from a baseline using near-storm environmental conditions (Brotzge et al. 2013; Anderson-Frey and Brooks 2021). In addition, Gibbs and Bowers (2019) found that while velocity signatures in supercells can help distinguish between weak and significant tornadoes (rated at least EF2 on the enhanced Fujita scale), the same does not apply to QLCSs. One potential opportunity to address these challenges is to further incorporate dual-polarization (dual-pol) radar data into the warning decision process through the mesovortex warning system. Dual-pol data can provide important information about processes that impact mesovortex development and strength, such as descending rear-inflow jets, downdraft characteristics, and updraft characteristics. The associated dual-pol signatures may be able to provide additional information about mesovortex tornado potential and possibly increase confidence in the issuance of a tornado warning. However, most dual-pol radar signatures, as well as some potentially helpful single-polarization signatures, are not currently incorporated into the mesovortex warning system.

Therefore, the purpose of this study is to examine the evolution of two single- and four dual-pol radar signatures—with the primary focus being on the dual-pol signatures—that might provide useful information to forecasters regarding mesovortex development as well as severe wind and tornado potential. Specifically, we aim to explore which, if any, radar signatures are commonly present with tornadic and nontornadic mesovortices, precede mesovortex development, or provide an indication of mesovortex strength and impacts. A special focus was placed on the last point since anticipating if a given mesovortex will produce wind damage and/or a tornado is one of the biggest challenges facing warning forecasters during QLCS events. If any radar signature does provide information regarding these factors, it could be added as a confidence builder to the mesovortex warning system. To address these questions, we first considered dual-pol data in the context of conceptual models and the mesovortex warning system (section 2) and then quantified the evolution of various dual-pol radar signatures of 167 QLCS mesovortices (section 4). We also quantified the evolution of two single-polarization radar signatures that can be used by NWS forecasters (section 5) and compared all radar signatures to near-storm environmental information (section 6), as well as the range from the nearest radar (section 7).

2. QLCS conceptual models, the mesovortex warning system, and dual-pol radar signatures

QLCS conceptual models are based on years of research and are a key part of successful warning decision-making (Andra et al. 2002). Previous works examining potential sources of vertical vorticity and mechanisms of mesovortex formation help provide information that can guide the development of such conceptual models (e.g., Wheatley and Trapp 2008; Atkins and St. Laurent 2009; Conrad and Knupp 2019; Flournoy and Coniglio 2019; Marion and Trapp 2021; Fischer and Dahl 2022). However, uncertainty remains regarding what mechanisms are most important for mesovortex development, and these mechanisms might vary across environments and at different times during storm evolution (e.g., Sherburn and Parker 2014; Flournoy and Coniglio 2019; Fischer and Dahl 2022; Goodnight et al. 2022). This uncertainty motivates recent research, such as the Propagation, Evolution, and Rotation in Linear Storms (PERiLS) field project, that could support even stronger scientific conceptual models. For now, our understanding points toward several features that likely play a role in mesovortex development, including rear-inflow jet surges, tilting of vorticity by a downdraft, tilting and stretching of vorticity by an updraft, and horizontal shearing instability.

Weather radar can provide insights into many of these processes and is critical to the mesovortex warning system (NWS 2023). For example, one important feature within the mesovortex warning system is a surge or bow in the convective line observed via radar reflectivity and velocity data. Atkins and St. Laurent (2009) found that a surge in the gust front enhances low-level convergence and updraft strength, which increases low-level stretching of vorticity. Additionally, Flournoy and Coniglio (2019) found that a rear-inflow jet surge caused more rapid tilting of horizontal vorticity within mesovortex air parcels that originated in the storm inflow. Radar confidence builders and nudgers within the mesovortex warning system, such as a reflectivity tag or cell merger, can indicate the potential for a locally stronger updraft, while others, such as a rear inflow notch or reflectivity line break, can indicate the existence of a descending rear-inflow jet and downdrafts (WDTD 2020; NWS 2023). Many previous studies mentioned above discuss the importance of downdrafts and updrafts in mesovortex development. Indeed, the presence of more confidence builders, such as those described above, has been shown to increase skill in predicting tornadic mesovortex development (Gibbs 2021).

Many of the existing radar signatures within the mesovortex warning system are connected to previous QLCS work and existing conceptual models. If any dual-pol signature were incorporated into the system, it should also be connected to processes identified in previous work and existing conceptual models that are relevant to mesovortex development and strength. Potential signatures identified for our analysis include localized reductions in specific differential phase (K_{DP}) referred to as K_{DP} drops, mid- and low-level K_{DP} cores, and differential reflectivity (Z_{DR}) columns. For review, Z_{DR} is an indicator of the shape of the dominant hydrometeors and is generally higher for increasing raindrop sizes, while K_{DP} is an indicator of the liquid water content within a radar volume (e.g., Kumjian 2013). Each radar signature and its possible connection to important processes are described in more detail below.

a. K_{DP} drops

A K_{DP} drop is an area of reduced ($<0.5^\circ$ km^{-1}) K_{DP} behind the leading edge of the QLCS and is collocated with

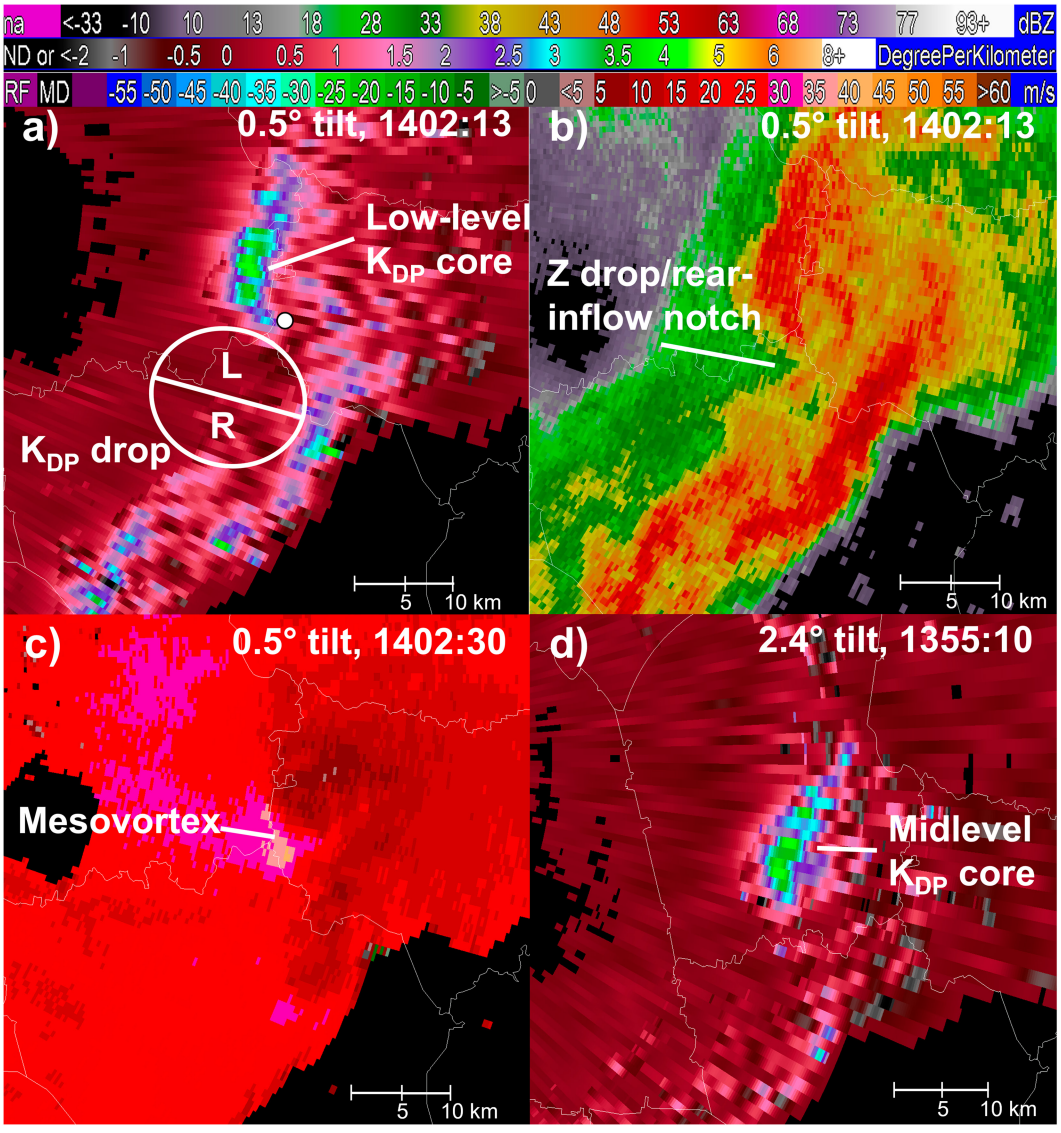

FIG. 1. Example of (a) a K_{DP} drop roughly divided into left and right halves, (b) corresponding reflectivity (Z) drop and rear-inflow notch, (c) corresponding mesovortex depicted in ground-relative 0.5° elevation angle radial velocity, and (d) a midlevel K_{DP} core all occurring on 1 Mar 2017 in middle Tennessee. The white dot in (a) marks the approximate location of the mesovortex shown in (c). Reflectivity, K_{DP}, and velocity color bars are included at the top. North is toward the top of each image.

the rear-inflow jet (Fig. 1a; see the animation in the online supplemental material). It likely develops in response to evaporation (e.g., Sachidananda and Zrnić 1987; Kumjian and Ryzhkov 2008) caused by a descending rear-inflow jet and is similar in idea and location to the rear-inflow notch and reflectivity drop (Fig. 1b) within the mesovortex warning system. Since K_{DP} drops are likely associated with descending rear-inflow jets and rear-inflow jet surges, they could provide forecasters with another way to identify and even anticipate localized surges in the convective line, which are likely indicative of increased mesovortex potential (e.g., Atkins and St. Laurent 2009; Schaumann and Przybylinski 2012; Flournoy and Coniglio 2019). This idea could be especially true when the orientation of the rear-inflow jet is not favorable to the radar viewing angle, which makes the rear-inflow jet harder to identify using velocity data alone. The K_{DP} drops can also be clearer, more distinct, and potentially easier to identify than the related features in reflectivity because the dynamic range of K_{DP} is nearly an order of magnitude less than reflectivity, and K_{DP} is more sensitive to the evaporation of smaller raindrops than reflectivity (e.g., Kumjian and Ryzhkov 2008).

b. *Mid- and low-level K_{DP} cores*

A K_{DP} core is an area of $\geq 1.0°$ km^{-1} K_{DP} located near and below the environmental melting layer that is typically

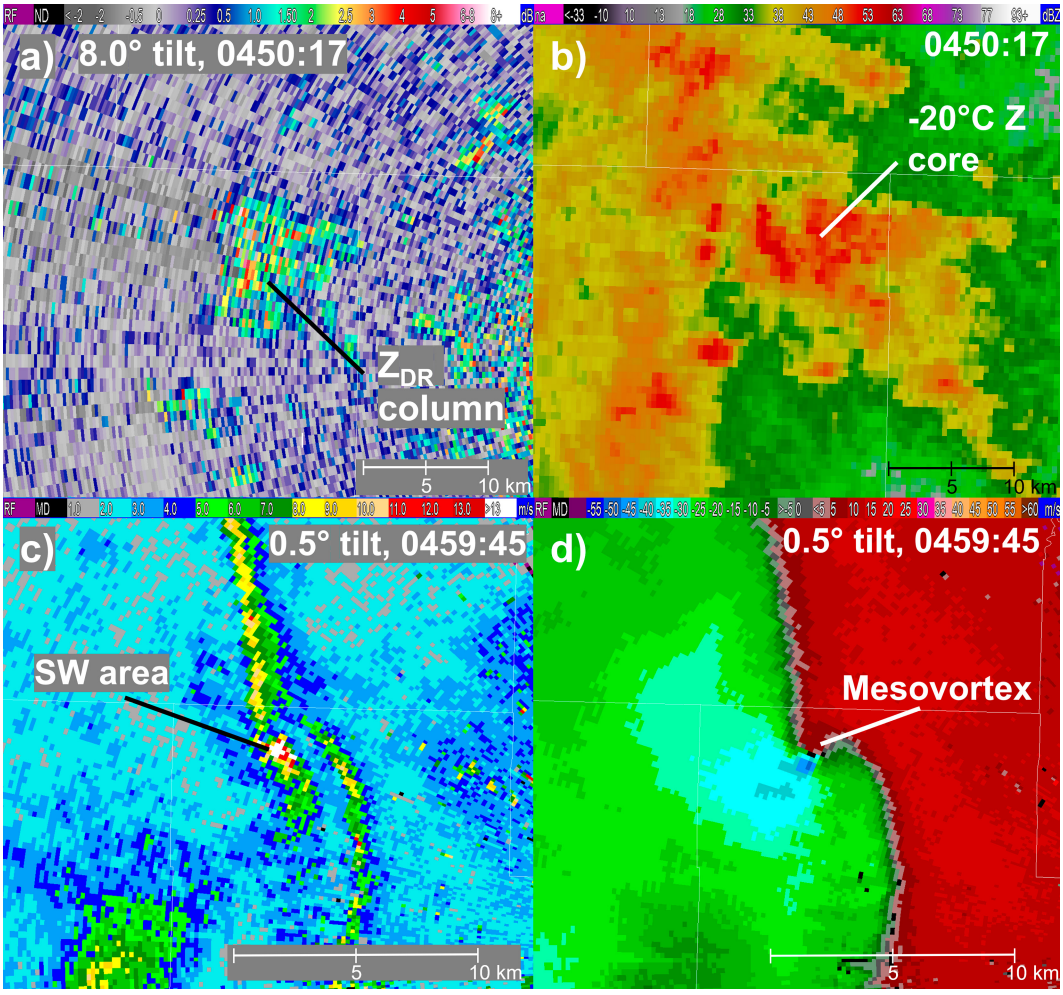

FIG. 2. Example of (a) a Z_{DR} column observed at the 8.0° elevation angle (~6.1 km above ground level), (b) a −20°C reflectivity (Z) core as depicted by the −20°C reflectivity field, (c) an area of enhanced low-level (0.5° elevation angle) spectrum width (SW), and (d) a mesovortex depicted in ground-relative 0.5° elevation angle radial velocity all occurring on 18 Jul 2015 in central Minnesota. North is toward the top of each image.

partially or completely surrounded by $K_{DP} < 1.0°\ km^{-1}$ (Figs. 1a,d; see animations in the supplemental material) and can be an indicator of processes controlling downdraft intensity, such as precipitation loading and melting (e.g., Hubbert et al. 1998; Kumjian et al. 2019; Kuster et al. 2021). A stronger K_{DP} core within or near a descending rear-inflow jet could indicate the presence of a stronger localized downdraft within that rear-inflow jet. A stronger downdraft would likely cause stronger outflow when it reaches the surface, which could result in a stronger rear-inflow jet surge within the convective line. This surge may lead to stronger low-level convergence along the updraft–downdraft convergence zone, a stronger low-level updraft, and enhanced tilting and stretching of existing vorticity (e.g., Atkins and St. Laurent 2009; Flournoy and Coniglio 2019; Boyer and Dahl 2020). These K_{DP} cores likely also indicate at least some cooling within the downdraft and, therefore, a larger low-level thermal gradient. Assuming the resulting outflow is not too cold, this cooling would increase baroclinic vorticity generation that could then be tilted and stretched by an updraft (e.g., McDonald and Weiss 2021). Observational studies of QLCSs have noted higher low- to midlevel (~0–4 km above ground level) K_{DP} with tornadic mesovortices when compared to K_{DP} in nontornadic mesovortices (Pardun 2023) and descent of a K_{DP} core prior to increased rotation at the 0.5° elevation angle or reports of severe wind (Loeffler 2017; Frugis 2020).

c. Z_{DR} columns

A Z_{DR} column is a vertically continuous area of $Z_{DR} \geq 1.0$ dB above the environmental melting layer that is partially or completely surrounded by $Z_{DR} < 1.0$ dB (Fig. 2a; see the animation in the supplemental material) and, similar to −20°C reflectivity cores (Fig. 2b, section 5a), is an indicator of updraft location and strength (e.g., Tuttle et al. 1989; Snyder et al. 2015). The Z_{DR} column characteristics, especially size, may provide information about tornado likelihood in supercells, with tornadic

supercells having larger and deeper Z_{DR} columns than those in nontornadic supercells (e.g., Van Den Broeke 2020; Wilson and Van Den Broeke 2021; Healey and Van Den Broeke 2023). Similarly, in QLCSs, the presence of a stronger and larger updraft could result in increased tilting and stretching of vorticity and an increased potential for mesovortex development (e.g., Boyer and Dahl 2020; Marion and Trapp 2021).

3. Radar data analysis and QLCS events

a. *Identifying events and classifying mesovortices*

We identified QLCS events for analysis using the Convective Warning Improvement Project's training content (NWS 2023), PERiLS cases, and recent QLCS events in central Oklahoma. All events included multiple tornado and severe wind reports. For all events, we defined a mesovortex as a rotational signature that extended through a depth of at least 2.4 km (8000 ft), persisted for at least two Weather Surveillance Radar-1988 Doppler (WSR-88D) volume scans (~8–10 min), and had a rotational velocity (sum of maximum inbound and outbound velocity divided by two) of at least 10 m s^{-1} (19.4 kt; e.g., Weisman and Trapp 2003; Thompson et al. 2012; Gibbs and Bowers 2019; Sessa and Trapp 2020; Gibbs 2021). Mesovortices also had to occur in an area of the QLCS roughly consistent with the three ingredients method (cold pool and ambient low-level shear are balanced or slightly shear dominant, 0–3-km line-normal bulk shear ≥ 15 m s^{-1}, and surge/bow in the line) since mesovortices are far less likely to occur in other areas of the QLCS and forecasters are far less likely to consider such areas for a tornado warning (Schaumann and Przybylinski 2012; Gibbs 2021; NWS 2023). In total, we analyzed 92 tornadic and 75 nontornadic mesovortices that occurred across 25 different days, every season of the year, varying instability and shear profiles (determined via 13-km Rapid Refresh (RAP) model output; section 6), and 16 states (Fig. 3, Table 1). All mesovortices and distinguishable radar signatures were within 165 and 177 km (89.1 and 95.6 n mi) of the nearest WSR-88D radar, respectively, with a large majority of both being within 150 km (81.0 n mi). For 22 of these days containing 157 mesovortices, radar data from the operational WSR-88D radar network were downloaded. For the remaining 3 days containing 10 mesovortices, S-band data from a research WSR-88D located in Norman, Oklahoma (KOUN), were used. Since KOUN is a research radar, operators can use customized volume coverage patterns (VCPs) and collect 90° sectors of data to obtain rapid-update volume scan times of ~1.1–1.9 min. The sample size of available data was too small to draw any meaningful conclusions regarding rapid- and traditional-update data, but we still used these data in our analysis because they represented the best available data for this small set of cases. For all K_{DP} signature analyses, K_{DP} was computed using the same method applied in NWS operations (WDTD 2011).

About 90% (n = 150) of the analyzed mesovortices were associated with "true" linear QLCSs as described in Gibbs (2021). We did not exclude mesovortices that appeared to be

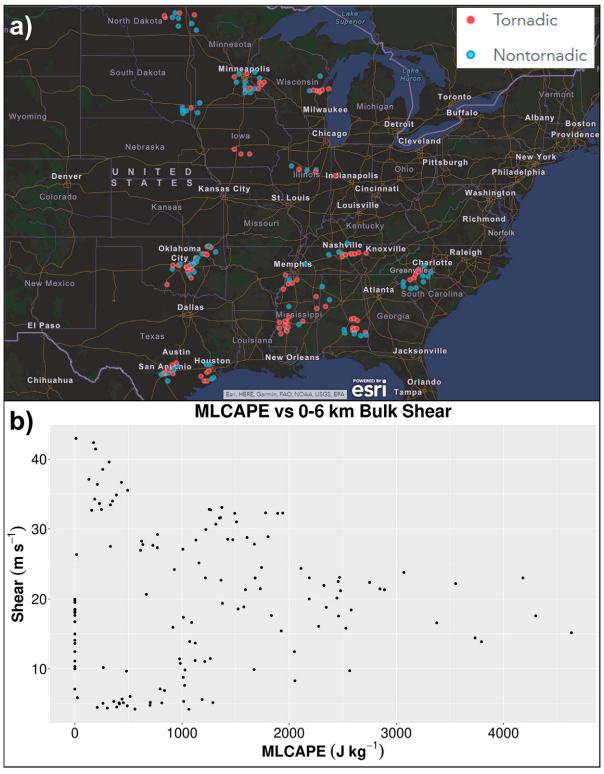

FIG. 3. (a) Approximate locations of all analyzed tornadic (red dots) and nontornadic (blue dots) mesovortices and (b) scatterplot of 0–6-km bulk shear vs MLCAPE for all mesovortices where environmental data were available (n = 162).

associated with the other submodes described in Gibbs (2021) or the two mesovortices that were likely associated with embedded supercells. As long as the mesovortex was within a linear storm mode (i.e., not a super- or multicell cluster) with features typically associated with QLCSs (e.g., rear-inflow jet), it was included in our analysis. It is likely important to account for storm mode, submode, and mode history since they are variables that could influence radar signature characteristics. However, assessing storm mode information adds another layer of potential subjectivity to any analysis, and the number of events falling outside of "true" linear was small in this study, so we decided not to subclassify our events.

We classified mesovortices based on information from the National Centers for Environmental Information's *Storm Data* publication (available online at https://www.ncdc.noaa.gov/stormevents/) and used these classifications as a basis for our analysis in sections 4–6. For example, a mesovortex that was associated (i.e., nearly collocated in space and time) with a tornado report was classified as "tornadic," whereas a mesovortex that was not associated with a tornado report was classified as "nontornadic." Similarly, a mesovortex that was associated with any severe wind report was classified as "damaging," whereas a mesovortex not associated with a severe wind report was classified as "nondamaging." These nontornadic and nondamaging mesovortices were considered the null events for this study, rather

TABLE 1. Case dates, states, and the number of mesovortices occurring on each day. KOUN cases occurred on 21 Oct 2017, 3 May 2018, and 11 Oct 2021.

Date; states affected	Tornadic mesovortices	Nontornadic mesovortices	Damaging mesovortices (wind or tornado report)	Nondamaging mesovortices (no report)
7 Aug 2013; WI	6	2	7	1
17 Nov 2013; IN	1	0	1	0
21 Dec 2013; AR, MS	5	2	7	0
22 Jul 2014; ND, MN	4	6	7	3
18 Jul 2015; MN, WI	3	6	6	3
6 Jul 2016; MN, WI	5	3	6	2
30 Nov 2016; SC	1	7	4	4
14 Feb 2017; TX	5	4	5	4
20 Feb 2017; TX	7	7	8	6
1 Mar 2017; TN; KY	7	4	10	1
30 Apr 2017; MS	10	3	11	2
6 Aug 2017; OK	4	3	5	2
31 Oct 2017; OK	1	0	1	0
23 Oct 2017; SC, NC	4	2	4	2
3 May 2018; OK	2	2	2	2
18 May 2019; OK	1	0	1	0
21 May 2019; OK	2	2	2	2
26 May 2019; OK	3	4	5	2
16 Jun 2019; IL	2	3	3	2
20 Aug 2019; IA	3	0	3	0
11 Sep 2019; IA, MN, SD	1	6	3	4
31 Mar 2020; AL	4	2	4	2
11 Oct 2021; OK	3	2	3	2
31 Mar 2022; AL	3	2	3	2
5 Apr 2022; AL	5	3	7	1
Total mesovortices	92	75	118	49

than radar signatures occurring without mesovortices, because anticipating mesovortex impacts is a current operational challenge, but this choice could limit conclusions about skillful mesovortex prediction. Any mesovortex that was associated with a wind report but not a tornado report was classified as "wind only." We also created classifications based on the reported enhanced Fujita (EF) scale rating of a tornado. Of course, there are limitations with *Storm Data* and the EF scale (e.g., Trapp et al. 2006; Edwards et al. 2013, 2021), but they do serve as the official record in the United States. This limitation does create a caveat to many of our conclusions since they depend on verification and it can be difficult to know the true severity or intensity of any given mesovortex. To avoid complete reliance on *Storm Data*, we also classified mesovortices based on the quartiles of radar-observed maximum 0.5° elevation-angle rotational velocity for each mesovortex. This method also has limitations, such as radar beam height and broadening, but it provides a more objective, quantitative measure of mesovortex intensity and potential impacts.

b. Radar signature analysis methods

We began radar signature analysis by identifying a mesovortex. All associated radar signatures were then located and tracked backward in time to each signature's initial development. Only one mesovortex was associated with each radar signature, except for K_{DP} drops, where a mesovortex could occur on the left and right sides of a single K_{DP} drop. We wanted all analysis methods to be readily available to forecasters today, so to quantify radar signature evolution, other than K_{DP} drops (section 4a), we used a cursor readout tool to determine each signature's maximum value at every volume scan between signature development time and signature dissipation or mesovortex dissipation time, whichever occurred first. The K_{DP} cores (section 4b) and Z_{DR} columns (section 4c) associated with four and three mesovortices, respectively, appeared to be present and nearly steady state for over an hour before the mesovortex developed (i.e., when rotational velocity first reached $\geq$10 m s^{-1}). Since it is unlikely that storm-scale processes specifically related to a single mesovortex would persist for over an hour, we trimmed the radar signature analysis time, to begin with the volume scan closest to 30 min prior to mesovortex development time. Ultimately, we compared the distributions of radar signature magnitudes using all volume scans (multiple values per mesovortex) and the overall maximum value (one value per mesovortex). Results were similar between the two methods, so here, we only show results for the overall maximum values (one value per mesovortex), since these values would likely be easiest to apply and most relevant to real-time warning operations. We used the Kolmogorov–Smirnov (K-S) test to determine if statistically significant differences existed between the full distributions of various classifications of mesovortices. Any p value < 0.05 was considered statistically significant. Since melting layer height is important in our analysis of K_{DP} cores and Z_{DR} columns, we approximated it using the height where Z_{DR} began to increase and the

TABLE 2. Number and percentage of all radar signatures associated with tornadic, nontornadic, and all mesovortices.

Radar signature	Number (%) for tornadic mesovortices	Number (%) for nontornadic mesovortices	Number (%) for all mesovortices
K_{DP} drop	86 (93.5%)	72 (96.0%)	158 (94.6%)
Midlevel K_{DP} core	72 (78.3%)	58 (77.3%)	130 (77.8%)
Low-level K_{DP} core	77 (83.7%)	63 (84.0%)	140 (83.8%)
Z_{DR} column	69 (75.0%)	60 (80.0%)	129 (77.3%)
−20°C reflectivity core	42 (45.7%)	34 (45.3%)	76 (45.5%)
Area of enhanced low-level spectrum width	82 (89.1%)	58 (77.3%)	140 (83.8%)

correlation coefficient began to decrease (e.g., Zrnić et al. 1993; Giangrande et al. 2008) and used wet-bulb zero height from nearby (as close as possible in time and space) observed soundings as additional verification.

For K_{DP} drops, we primarily performed a qualitative analysis because we expect the presence of the signature rather than its magnitude to be more important in an operational setting, especially since the minimum K_{DP} value within a K_{DP} drop is frequently at or near 0° km^{-1}. In addition, the identification and tracking of K_{DP} drops is more subjective than the other radar signatures. Its presence is easiest to identify by looping K_{DP}, reflectivity, and velocity images and searching for an area within the rear-inflow jet where K_{DP} decreases with time and "cuts into" the higher values of K_{DP} within the main convective line (Fig. 1a). This process, combined with an understanding of storm structure and evolution (e.g., location of rear-inflow jet and anticipation of bowing segments), helps in identification of the signature, but determining an exact start and end time is challenging, especially since K_{DP} naturally decreases everywhere behind the main convective line where lower rain rates typically exist.

We quantified the evolution of K_{DP} cores at the elevation angle closest to but below the environmental melting layer (referred to as midlevel K_{DP} cores) and at the 0.5° elevation angle (referred to as low-level K_{DP} cores). Beam height is important to consider for this distinction, since depending on melting layer height, the low-level K_{DP} core may not be sampled at farther ranges where the beam height is too high. For two mesovortices at long ranges, the 0.5° elevation angle was also the elevation angle closest to the melting layer, so we only quantified midlevel K_{DP} cores in those instances.

We quantified Z_{DR} column magnitude using multiple methods: 1) maximum Z_{DR} on the highest elevation angle with $Z_{DR} \geq 1$ dB, 2) maximum height of $Z_{DR} \geq 1$ dB above ground level (referred to as Z_{DR} column height), 3) maximum Z_{DR} on a constant-altitude plan position indicator (CAPPI) 5 km above ground level, and 4) maximum Z_{DR} on a CAPPI 2 km above the height of the environmental melting layer. For Z_{DR} column height, we measured height above ground level for ease of calculation during real-time warning operations, but height above the melting layer could also be used. However, this measurement would be easiest to make with the aid of an automated calculation (e.g., Snyder et al. 2015; Wilson and Van Den Broeke 2021), and such an algorithm is not currently operational. Similarly, we did not calculate Z_{DR} column area, despite previous work showing its utility in supercells (e.g., Van Den Broeke 2020; French and Kingfield 2021), because this quantity would be difficult to determine in real time without the aid of an algorithm, and we chose to focus our work on what can currently be applied in operations.

An area of enhanced low-level spectrum width consists of spectrum width ≥ 7 m s^{-1} (13.6 kt), is located at the 0.5° elevation angle, persists for at least two scans, and is nearly collocated with a mesovortex (Figs. 2c,d in the supplemental material). We considered lower values of spectrum width than Spoden et al. (2012) suggested from their analysis of tornadic storms to capture the weaker, nontornadic mesovortices in our dataset. Enhanced spectrum width collocated with mesovortices is not surprising since we expect this in areas where the turbulent motions within storm-scale circulations result in greater variance in the Doppler velocity values (e.g., Istok and Doviak 1986; Spoden et al. 2012).

4. Dual-pol radar signatures

a. K_{DP} drops

The K_{DP} drops preceded 94.6% of all mesovortices in this study (Table 2). There also was a preferred mesovortex development location relative to the K_{DP} drop. Mesovortices always developed on the periphery of the K_{DP} drop, not within it. This observation makes sense as we would not expect mesovortices to develop within the sinking air of a descending rear-inflow jet. In addition, when roughly dividing the K_{DP} drop in half, based on a five-volume-scan, radar-reflectivity estimate of storm motion, 75.4% of all mesovortices developed on the left side of the K_{DP} drop near the low-level K_{DP} core (section 4b), 19.2% of all mesovortices developed on the right side of the K_{DP} drop, and 5.4% of all mesovortices occurred without a K_{DP} drop (Fig. 1a, Table 3). This result may relate to previous observations of tornadoes typically occurring north of a bow echo's apex (e.g., Fujita 1981; Przybylinski 1995; Atkins et al. 2004). Since many mesovortices in this dataset were associated with K_{DP} drops and commonly developed in a similar location relative to the K_{DP} drop, this radar signature could increase forecaster confidence regarding the placement of warning polygons prior to mesovortexgenesis.

b. Mid- and low-level K_{DP} cores

Midlevel K_{DP} cores preceded 77.8% of all mesovortices in this dataset (Table 2). In general, midlevel K_{DP} cores tended to have higher magnitudes for tornadic mesovortices than

TABLE 3. Number and percentage of mesovortices developing on the left and right halves of a K_{DP} drop.

K_{DP} drop-relative position	Number (%) for tornadic mesovortices	Number (%) for nontornadic mesovortices	Number (%) for all mesovortices
Left	72 (78.3%)	54 (72.0%)	126 (75.4%)
Right	14 (15.2%)	18 (24.0%)	32 (19.2%)

nontornadic mesovortices, damaging mesovortices than nondamaging mesovortices, and mesovortices with higher rotational velocities (Fig. 4). Statistically significant differences (i.e., $p < 0.05$) existed between the midlevel K_{DP} core distributions of tornadic and nontornadic mesovortices, damaging and nondamaging mesovortices, and mesovortices with rotational velocities > 22.63 m s^{-1} (44.0 kt; 75th percentile) and those with rotational velocities ≤ 15.0 m s^{-1} (29.2 kt; 25th percentile; Fig. 4, Table 4). In this dataset, these rotational velocities are close to the observed median rotational velocities of mesovortices associated with EF1+ tornadoes and nontornadic mesovortices, respectively. To introduce a rough first look at an operationally relevant threshold for distinguishing mesovortex impacts, we used the 75th percentile of midlevel K_{DP} cores associated with nondamaging and nontornadic mesovortices as a starting point. In this dataset, those values are 4.89° and 5.24° km^{-1}, respectively. Therefore, if a midlevel K_{DP} core reaches a maximum value of about 4.90° or 5.25° km^{-1}, a forecaster could have increased confidence that an existing mesovortex will produce wind damage or a tornado, respectively. These thresholds also fall below the median K_{DP} core magnitude for damaging and tornadic mesovortices, which would help minimize the number of missed events (Fig. 4).

We used maximum values of K_{DP} to set a potential foundation for rough operationally relevant thresholds that can help in anticipating mesovortex impacts, but K_{DP} core magnitude trends over time are another crucial piece of information. We therefore quantified trends by grouping K_{DP} core magnitudes for all tornadic and nontornadic mesovortices into half-minute intervals, relative to mesovortex development, extending from when the signature developed to when it dissipated (and not exceeding 30 min before or after mesovortex development). These bins of K_{DP} core evolution were then plotted using a rolling average of seven half-minute intervals (3.5 min). This rolling average was chosen to reduce short-term variability while preserving data that forecasters might be likely to revisit once or twice during a volume scan (i.e., every 3–5 min). We also produced box plots at 5-min intervals to provide more information

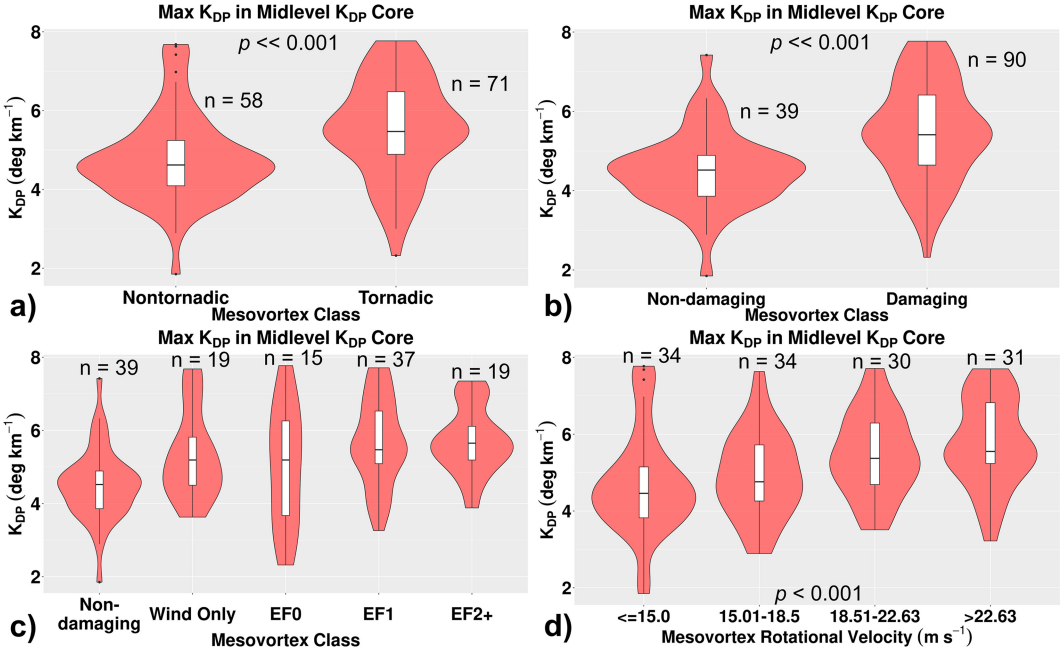

FIG. 4. Violin plots of midlevel K_{DP} core maximum values for (a) tornadic and nontornadic mesovortices, (b) damaging and nondamaging mesovortices, (c) mesovortices classified by their associated severe weather reports or tornado EF scale ratings, and (d) mesovortices classified by the quartiles of their maximum observed 0.5° elevation angle rotational velocities. The red area shows the probability density with a greater width indicating a higher frequency of occurrence. Associated box plots are included within each violin plot for reference. Box edges are the lower (Q1) and upper (Q3) quartiles, the horizontal black line is the median, and outliers are indicated by black dots. K-S test p values and a number of mesovortices (n) used to create each violin plot are also included. In (c), no p values are included, and in (d), the p value is for the highest and lowest category of rotational velocity.

TABLE 4. Statistical significance for each radar signature and various measures of mesovortex intensity and impacts. The p values less than 0.05 are considered statistically significant and are in bold; p values < 0.0001 are indicated as ≪0.001.

Radar signature	Tornadic vs nontornadic p value	Damaging vs nondamaging p value	EF2+ vs EF0 p value	>22.63 vs ≤15.0 m s^{-1} rotational velocity p value
Midlevel K_{DP} core	**≪0.001**	**≪0.001**	0.26	**≪0.001**
Low-level K_{DP} core	**≪0.001**	**≪0.001**	**0.02**	**<0.001**
Z_{DR} column height	0.65	0.26	0.99	0.13
−20°C reflectivity core	0.15	**0.04**	0.84	0.13
Area of enhanced low-level spectrum width	**<0.001**	**0.03**	0.50	**≪0.001**
Rotational velocity	**≪0.001**	**<0.001**	**<0.001**	—

about how the K_{DP} core magnitude distribution changed over time. One caveat for all of the trend analyses is that sample sizes are relatively small (i.e., <5–10), especially at times greater than 20 min from mesovortex development. For midlevel K_{DP} cores, there were no obvious differences in the trends of tornadic and nontornadic mesovortices (Fig. 5a). The clearest differences between tornadic and nontornadic mesovortices over time were confined to the K_{DP} core magnitudes. The median K_{DP} core magnitude of tornadic mesovortices nearly matched or exceeded the upper-quartile K_{DP} core magnitude of nontornadic mesovortices beginning 20–25 min prior to mesovortex development and continuing to 25–30 min after mesovortex development (Fig. 5b). The median time between midlevel K_{DP} core development and mesovortex development was 14.3 min, so not all events had a K_{DP} core 20–25 min before mesovortex development. However, in general, when the K_{DP} core developed and as it evolved, it was stronger for tornadic mesovortices than nontornadic ones.

Low-level K_{DP} cores were associated with 83.8% of all mesovortices in this dataset (Table 2). Similar to midlevel K_{DP} cores, low-level K_{DP} cores tended to be stronger for tornadic mesovortices than nontornadic mesovortices, damaging mesovortices than nondamaging mesovortices, mesovortices associated with tornadoes rated higher on the EF scale, and mesovortices with stronger rotational velocities (Fig. 6). Statistical significance was observed for the same categories as

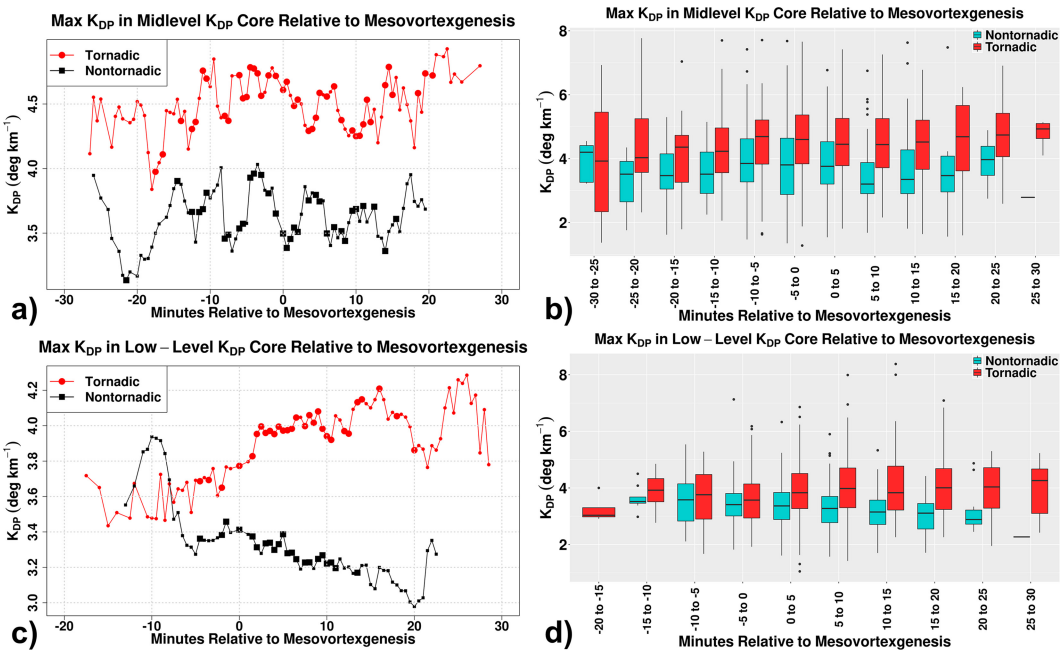

FIG. 5. Time series of maximum (a) midlevel K_{DP} core magnitude and (c) low-level K_{DP} core magnitude and box plots of maximum (b) midlevel K_{DP} core magnitude and (d) low-level K_{DP} core magnitude over time. In (a) and (c), the red line indicates tornadic mesovortices, and the black line indicates nontornadic mesovortices. The larger marker sizes in (a) and (c) indicate a sample size of ≥5 and 10 scans, respectively. A seven-time-step rolling average is plotted for each 0.5-min interval (dots). In (b) and (d), red boxes indicate tornadic mesovortices, and light blue boxes indicate nontornadic mesovortices. Box edges are the lower (Q1) and upper (Q3) quartiles, the horizontal black line is the median, and outliers are indicated by black dots.

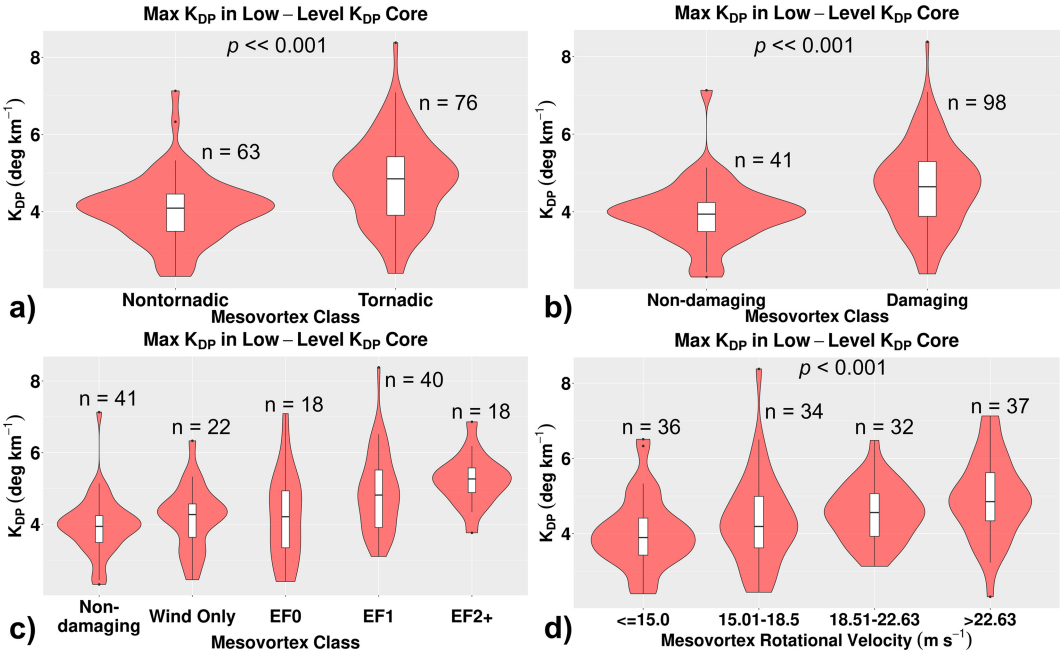

FIG. 6. As in Fig. 4, but for low-level K_{DP} cores.

midlevel K_{DP} cores, but statistically significant differences also existed between the low-level K_{DP} core distributions of tornadoes rated EF2+ and those rated EF0 (Table 4). Using the same method as midlevel K_{DP} cores, a rough threshold for discriminating between damaging and nondamaging mesovortices and tornadic and nontornadic mesovortices for low-level K_{DP} cores is 4.3° and 4.5° km^{-1}, respectively. Low-level K_{DP} cores are also the only radar signature we analyzed where this threshold (i.e., 4.5° km^{-1}) also lies above the median for EF0 tornadoes and below the 25th percentile of EF2+ tornadoes (Fig. 6). Therefore, low-level K_{DP} cores may be one of the more helpful radar signatures in distinguishing between mesovortices that produce stronger and weaker tornadoes as well as stronger and weaker mesovortices overall though additional studies with larger sample sizes are needed to verify this result.

Unlike midlevel K_{DP} cores, low-level K_{DP} cores generally developed much closer to the time of mesovortex development, with a median time between low-level K_{DP} core development and mesovortex development of 2.1 min. However, distinctly different trends existed between tornadic and nontornadic mesovortices. In general, for tornadic mesovortices, low-level K_{DP} core magnitude increased from about −8 to +15 min around mesovortex development time, but for nontornadic mesovortices, it generally decreased from about −10 to +20 min around mesovortex development time (Fig. 5c). One caveat to this idea is the smaller sample sizes that exist at longer times prior to mesovortex development since 75% of low-level K_{DP} cores developed 5.7 min or less prior to mesovortex development. However, an intensifying low-level K_{DP} core could help build forecaster confidence in the likelihood of a tornadic mesovortex whereas a weakening low-level K_{DP} core could build confidence in a nontornadic mesovortex. While low-level K_{DP} cores would be sampled several times before mesovortex and especially tornado development, assuming Supplemental Adaptive Intravolume Low-Level Scanning (SAILS; Chrisman 2013) was running, the ability to see these trends in real time could be limited by slower radar update times. In addition to trends, the magnitude of the low-level K_{DP} core could also increase confidence, especially around and after mesovortex development time, during which period the median K_{DP} core magnitude of tornadic mesovortices exceeded the upper-quartile K_{DP} core magnitude of nontornadic mesovortices (Fig. 5d).

c. Z_{DR} columns

The Z_{DR} columns preceded 77.3% of all mesovortices by a median time of 16.6 min in this dataset, but unlike K_{DP} cores, we found no statistically significant differences between the Z_{DR} columns of various mesovortex classifications for any of the methods used to measure Z_{DR} column magnitude, so we only show Z_{DR} column height for simplicity (Fig. 7; Tables 2 and 4). The lack of statistically significant differences did not change even when we accounted for the range from the radar and environmental instability or used Z_{DR} column height above the melting layer rather than above ground level (not shown). We also did not see any clear differences in the trends of Z_{DR} column height between tornadic and nontornadic mesovortices, and the distributions of each mesovortex classification were relatively similar at nearly all time steps (Figs. 8a,b).

The lack of differences in Z_{DR} column magnitude across mesovortex classifications may relate to what Z_{DR} columns can tell us about updraft characteristics. Low-level (i.e., below 2 km) updraft strength is likely most important in QLCS

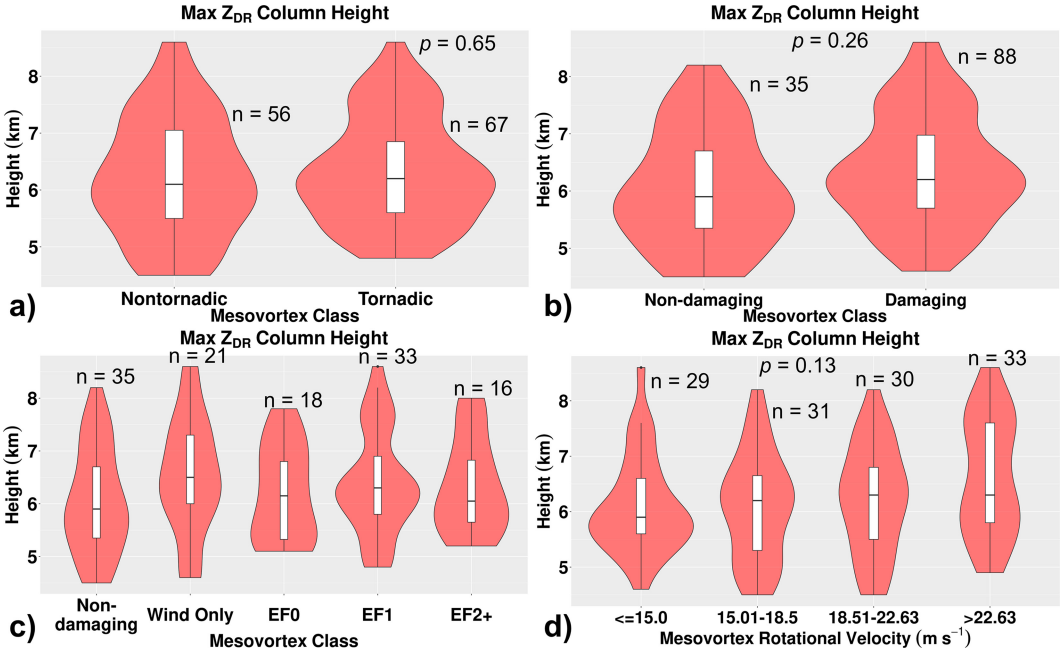

FIG. 7. As in Fig. 4, but for Z_{DR} column height.

mesovortexgenesis (e.g., Marion and Trapp 2021), whereas Z_{DR} columns may be more related to thermodynamically driven midlevel updraft strength (e.g., Kumjian et al. 2014; Snyder et al. 2015). Therefore, we expect that Z_{DR} columns may be useful in building confidence in which portions of the QLCS have the strongest updrafts and may be most likely to produce mesovortices but likely cannot be used to anticipate mesovortex strength or help distinguish which warning type, if any, is most appropriate.

5. Single-polarization radar signatures

We also examined single-polarization radar signatures not explicitly referenced within the mesovortex warning system using the same analysis methods used with dual-pol radar signatures.

a. Reflectivity cores at the −20°C altitude

Forecasters frequently use upper-level reflectivity cores to diagnose a storm's relative updraft strength, so they are also potentially relevant in anticipating mesovortex development (e.g., Witt et al. 1998; Kumjian et al. 2014). In this study, we used a reflectivity threshold of 50 dBZ to identify and quantify high-reflectivity cores at the −20°C altitude (Fig. 2b; supplemental material). We found that 50+ dBZ −20°C reflectivity cores were not a reliable mesovortex precursor signature, at least in this dataset. Only 45.5% of all mesovortices were associated with a 50+ dBZ −20°C reflectivity core (Table 2). There were no statistically significant differences between the reflectivity cores of tornadic and nontornadic mesovortices, but there were between damaging and nondamaging mesovortices (Fig. 9; Table 4). The much lower sample sizes compared to other radar signatures also prevented us from making any conclusions regarding trends over time. The use of 50 dBZ as a threshold for −20°C reflectivity cores likely led to the small percentage of mesovortices having this radar signature, and we expect that a lower threshold would result in a higher percentage. Investigation of lower thresholds may be worthy of future work, but with our focus on dual-pol signatures and the expectation that lower thresholds

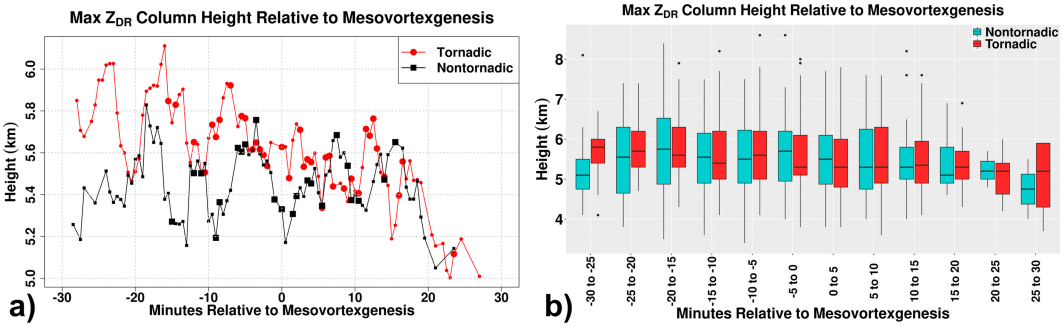

FIG. 8. As in Fig. 5, but for maximum Z_{DR} column height. The larger marker sizes in (a) indicate a sample size of ≥5 scans.

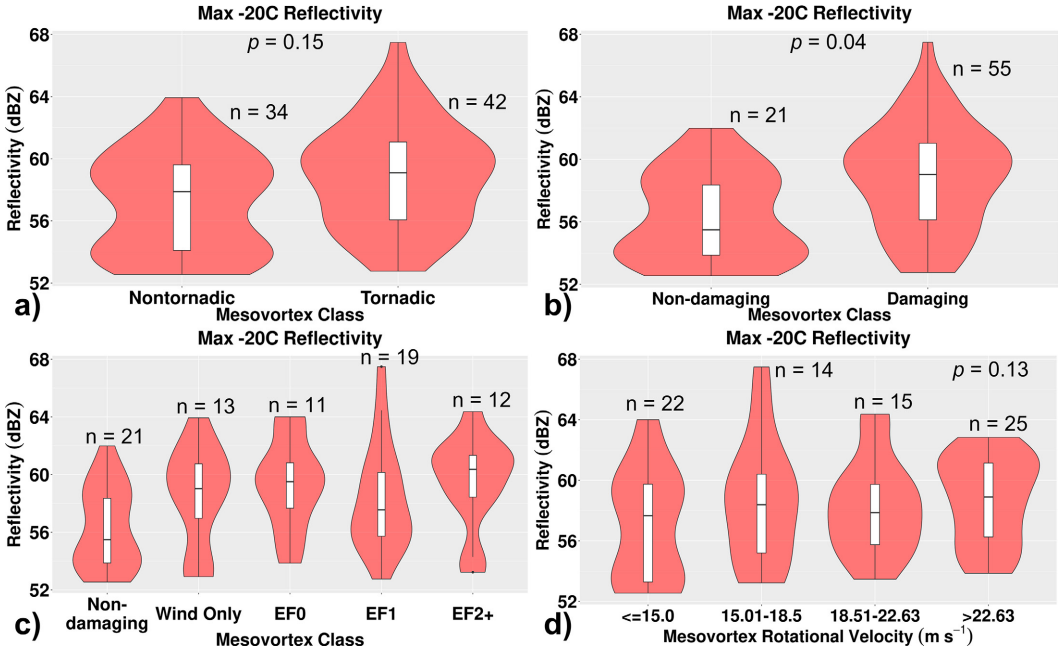

FIG. 9. As in Fig. 4, but for −20°C reflectivity cores.

would very likely not result in statistical significance near that seen with K_{DP} cores, we decided to not investigate lower thresholds here.

b. Area of enhanced low-level spectrum width

We found that areas of enhanced low-level spectrum width were associated with 83.8% of the mesovortices in this dataset (Table 2). In general, low-level spectrum width tended to be statistically significantly higher for tornadic mesovortices than nontornadic mesovortices, damaging mesovortices than nondamaging mesovortices, and mesovortices with stronger rotational velocities (Fig. 10; Table 4). However, unlike K_{DP} cores, maximum spectrum width was not greater for wind only versus nondamaging mesovortices and did not increase as tornado EF scale rating increased (Fig. 10c). These less pronounced differences in the distributions across different mesovortex classifications prevented us from suggesting a rough threshold to use for areas of enhanced low-level spectrum width.

As expected, the median time between the development of the area of enhanced low-level spectrum width and the mesovortex was 0.0 min. Spectrum width trends between tornadic and nontornadic mesovortices were also similar, with both increasing quickly in the few minutes before and after mesovortex development and then slowly decreasing with time after reaching the peak magnitude (Fig. 11a). Spectrum width was higher for tornadic mesovortices than nontornadic mesovortices at all times, but those differences were less pronounced than those observed with K_{DP} cores (Figs. 5 and 11b).

6. Environmental data and radar signatures

Another important aspect of anticipating storm mode, storm intensity, and mesovortex development is the consideration of near-storm environmental conditions (e.g., James and Markowski 2010; Schaumann and Przybylinski 2012; Thompson et al. 2012). We therefore used 13-km RAP model output to compare the magnitudes of various environmental parameters used in operations [e.g., mixed-layer convective available potential energy (MLCAPE), 0–3-km bulk shear, 0–3-km storm-relative helicity] to the magnitudes of the analyzed radar signatures. When available (n = 162), we extracted RAP data from a single point in time and location that was in proximity to each analyzed mesovortex and ahead of the cold pool (i.e., generally about 20 km to the east or east southeast of the mesovortex). In general, we did not find many significant differences or obvious relationships between radar signature magnitude and the analyzed near-storm environment parameters in this dataset. It is possible that radar signature magnitude is not strongly connected to environmental shear or instability. It is also possible that convective contamination in the RAP data affected the observed lack of relationships though we also did not observe many differences when looking at RAP data for 1 and 2 h prior to mesovortex presence. More studies with larger sample sizes are needed to investigate potential connections between near-storm environment and radar signature magnitude.

There were two exceptions to the limited number of relationships between environmental parameters and radar signatures. We observed stronger and taller Z_{DR} columns in environments with larger buoyancy (e.g., higher mixed-layer CAPE and higher 0–3 km CAPE). This result is not surprising given that previous work has noted a relationship between Z_{DR} columns and updraft strength (e.g., Kumjian et al. 2014), but it might have limited operational utility since Z_{DR} column magnitude does not appear to be related to mesovortex intensity or impacts (Fig. 7). We also observed stronger mesovortex

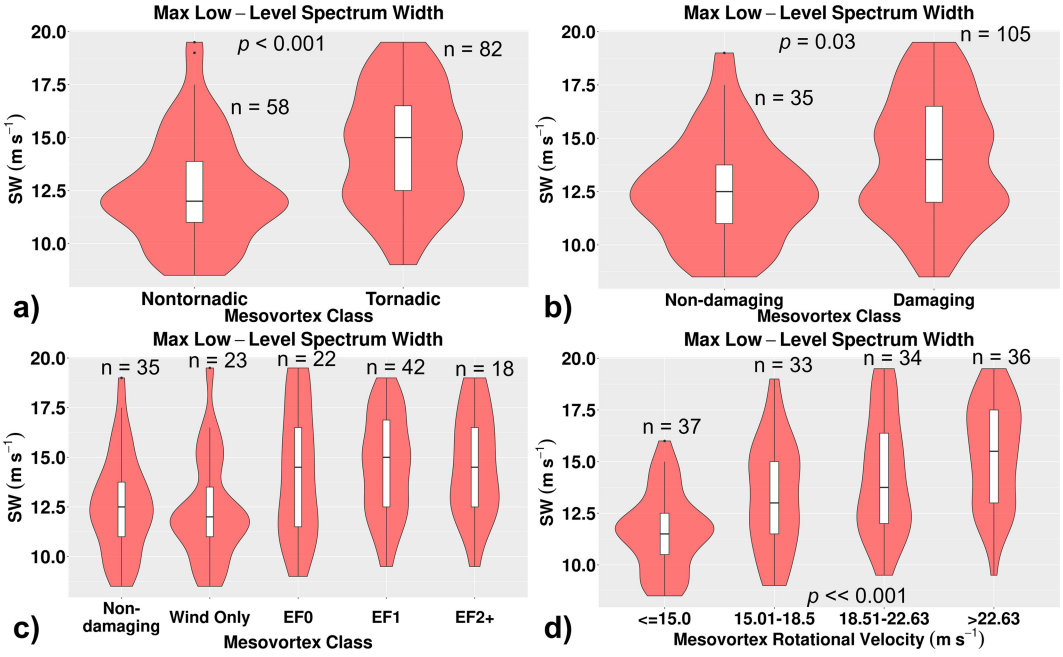

FIG. 10. As in Fig. 4, but for maximum low-level spectrum width.

rotational velocity in environments with stronger shear (e.g., higher 0–1-km bulk shear and effective storm-relative helicity). This result is also consistent with previous work (e.g., Thompson et al. 2012; Smith et al. 2015).

7. Range from the nearest radar

As the range from the radar increases, what can be resolved in radar data changes because beam height and width increase with range. For example, at longer ranges, the radar beam is higher above the ground, and the resolution is coarser, so observing small-scale features close to the ground becomes more challenging or impossible. We therefore examined the impact of range on radar signature magnitude by comparing tornadic and nontornadic mesovortices that occurred only beyond various range thresholds.

For midlevel K_{DP} cores, statistically significant differences between tornadic and nontornadic mesovortices always existed for mesovortices at closer ranges (i.e., within 90 km, 48.6 n mi). As we removed these close-range mesovortices, statistical significance began to decrease and disappear. For midlevel K_{DP} cores, when we only considered mesovortices beyond 90 km in range, statistically significant differences between tornadic and nontornadic mesovortices were nearly present (i.e., p value just above the 0.05 threshold) and clearly no longer present when looking only at mesovortices beyond 100 km (54.0 n mi) in range (Fig. 12). For low-level K_{DP} cores, statistically significant differences between tornadic and nontornadic mesovortices were present at all ranges though sample sizes were small beyond 100 km in range (not shown). For areas of enhanced low-level spectrum width, statistically significant differences were no longer present when we only considered mesovortices beyond 70 km (37.8 n mi; not shown). This observation suggests that spectrum width magnitude within mesovortices is sensitive to changes in radar beam height and width and may only be a useful radar signature for storms within ~70 km of the nearest radar. For Z_{DR} columns and −20°C reflectivity cores, we found no

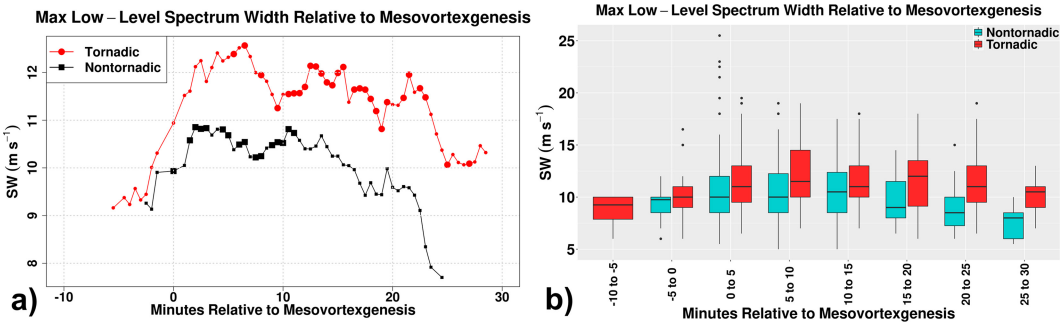

FIG. 11. As in Fig. 5, but for maximum low-level spectrum width. The larger marker sizes in (a) indicate a sample size of ≥10 scans.

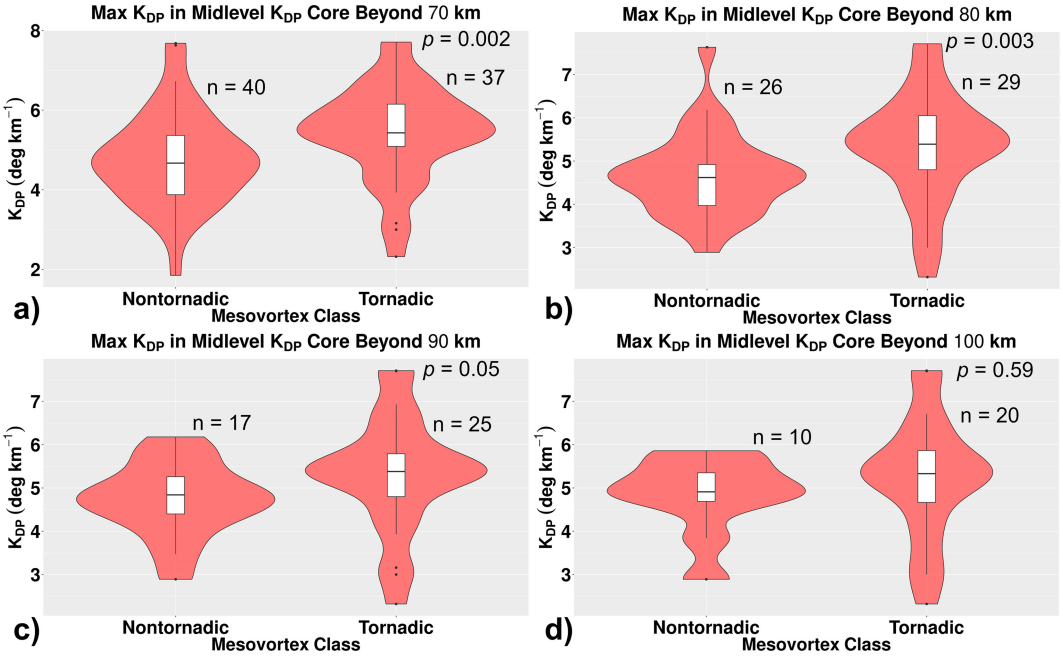

FIG. 12. Violin plots of midlevel K_{DP} core maximum values for mesovortices only at ranges greater than (a) 70 km (37.8 n mi), (b) 80 km (43.2 n mi), (c) 90 km (48.6 n mi), and (d) 100 km (54.0 n mi). The violin and box plot convention is the same as in Fig. 4.

statistically significant differences regardless of the range threshold used.

Range from the radar did not significantly affect the likelihood that a given signature was present with a mesovortex. For example, a low-level K_{DP} core was associated with 83.8% of all mesovortices (Table 2), 86.3% of all mesovortices ≥ 70 km (37.8 n mi) from the nearest radar, and 80.8% of all mesovortices ≥ 100 km (54.0 n mi) from the nearest radar. These results suggest that several of the radar signatures analyzed here can help a forecaster anticipate that a mesovortex is about to develop or is ongoing regardless of range (at least up to 150 km) from the nearest radar, but they become less useful at helping a forecaster anticipate the potential strength and impacts of a mesovortex as range increases, especially beyond 90 km (48.6 n mi). Since many mesovortices occur beyond a range of 90 km from the nearest radar, more work is needed to expand upon our relatively small sample size (n = 40) of mesovortices beyond 90 km and determine if any relationships exist between radar signature magnitude and mesovortex strength at these longer ranges.

Another consideration is the varying beam heights for a given elevation angle as the range from the radar changes. This effect may be especially relevant for radar signatures observed at the 0.5° elevation angle where beam height can range from less than 0.5 km for mesovortices close to the radar to over 1.5 km for mesovortices farther from the radar. For example, the ability to accurately determine mesovortex rotational velocity may be limited at greater ranges since maximum mesovortex strength tends to occur in the lowest 1 km above ground level (e.g., Atkins et al. 2004; Wheatley and Trapp 2008). In addition, tornadic mesovortices tend to be deeper than nontornadic mesovortices (e.g., Atkins et al. 2004), so it may be easier to detect tornadic than nontornadic mesovortices at longer ranges. To examine the potential impact of range on radar signature magnitude, we compared the maximum radar signature magnitude to the median radar signature range from the radar. In this dataset, there were no significant range impacts for any analyzed signature (not shown). However, additional research with a larger sample size that quantifies radar signature magnitude at various heights above ground level is needed to investigate the impacts of range on QLCS radar signatures.

8. Summary

Our research goals include identifying radar signatures, especially in dual-pol data, that can build upon and potentially be incorporated as additional confidence builders in the mesovortex warning system, to ultimately help forecasters anticipate mesovortex development and potential impacts. Through an analysis of 167 mesovortices across 25 different days and 16 states, we offer the following conclusions:

1) The K_{DP} drops likely precede a majority of mesovortices and provide an initial indication of where a mesovortex might develop if one were to develop. In our dataset, 94.6% of mesovortices are preceded by a K_{DP} drop, and 75.4% of mesovortices developed on the left half of the K_{DP} drop. They are similar in location and concept to the reflectivity drop and rear-inflow notch in the mesovortex warning system but tend to be more easily detectable than comparable features in reflectivity.

2) Midlevel K_{DP} cores likely provide useful predictive information about mesovortex development and intensity. In our dataset, 77.8% of mesovortices are preceded by midlevel K_{DP} core development by a median time of 14.3 min. Midlevel K_{DP} cores are also stronger for tornadic and damaging mesovortices as well as for mesovortices with higher low-level rotational velocities. In general, for this dataset, a midlevel K_{DP} core magnitude of $\geq 4.9^{\circ}$ km^{-1} may be a good starting point for distinguishing between mesovortices that are more likely to produce damage (Fig. 4).
3) Low-level K_{DP} cores provide less predictive information than midlevel K_{DP} cores but still likely provide helpful diagnostic information about mesovortex intensity and potential impacts. In our dataset, low-level K_{DP} cores are stronger for all categories of more impactful mesovortices (e.g., tornadic vs nontornadic) but develop at about the same time as the mesovortex. In general, for this dataset, a low-level K_{DP} core magnitude of $\geq 4.3^{\circ}$ km^{-1} may be a good starting point for distinguishing between mesovortices that are more likely to produce damage (Fig. 5). Trends in low-level K_{DP} core magnitude were also different between tornadic and nontornadic mesovortices, so a consistently strengthening low-level K_{DP} core could build forecaster confidence in mesovortex tornado potential.
4) The Z_{DR} columns likely do not provide much useful information about mesovortex intensity. In our dataset, there are no significant differences in Z_{DR} column magnitude for any of the mesovortex intensity classifications. It is possible that Z_{DR} columns do not provide information about low-level updraft strength, which is probably most relevant for mesovortex development and intensity.
5) Reflectivity cores at the -20°C level may provide limited information about mesovortex intensity (i.e., differences existed between damaging and nondamaging mesovortices), but our reflectivity threshold of 50 dBZ is likely too high for QLCS events, so more work on this radar signature is needed.
6) Areas of enhanced low-level spectrum width probably provide some diagnostic information about mesovortex intensity when located within 70 km (37.8 n mi) of a radar but provide less information about mesovortex intensity than low-level K_{DP} cores. We suggest using this signature to help identify developing mesovortices, since 83.8% of mesovortices in our dataset are associated with this signature, but relying more on low-level K_{DP} cores and rotational velocity to diagnose mesovortex intensity.
7) Radar signature range from the nearest radar is important. In our dataset, as range increases, especially beyond 90 km (48.6 n mi), there are fewer notable differences between the radar signature magnitudes of tornadic and nontornadic mesovortices. However, the frequency of observing the radar signatures is much less impacted by increasing range. A larger sample size is needed, but this result suggests that these radar signatures may be helpful in anticipating mesovortex development and/or existence regardless of range from the radar (at least up to 150 km) but might be less helpful in anticipating mesovortex intensity at longer ranges.
8) The following is a characteristic timeline of radar signatures observed in this dataset: the midlevel Z_{DR} column and K_{DP} core develop first, typically around 15 min prior to the mesovortex (Figs. 13a,b). Several minutes later, the first low-level signature, the K_{DP} drop, develops (Fig. 13c). The low-level K_{DP} core then develops but only typically 0.5–5 min before the area of enhanced low-level spectrum width and mesovortex develop (Figs. 13c,e,f). For tornadic mesovortices, the tornado develops about 4.2 min after mesovortex development (median time in our dataset).

Our results suggest that several of these radar signatures, especially K_{DP} cores, can increase forecaster confidence in anticipating mesovortex development and intensity especially if incorporated into conceptual models such as the mesovortex warning system. Specifically, K_{DP} drops and K_{DP} cores appear to be related to localized surges in the convective line, which are a key component of the mesovortex warning system and in anticipating mesovortex development (e.g., Flournoy and Coniglio 2019; Gibbs 2021; Ungar and Coniglio 2023).

It is important to remember that none of these radar signatures can act as stand-alone indicators for a warning decision and the K_{DP} core thresholds mentioned above are simply initial starting points for consideration. In addition, the radar signatures studied here can occur without a mesovortex (i.e., null event). Though an initial look at our dataset suggests these null events are not common in areas where the three ingredients are met, their presence does limit how much we can conclude about the effectiveness of using these radar signatures to anticipate mesovortexgenesis. Future work, including the development of a robust sample of null events and an assessment of their characteristics relative to the three ingredients method, is needed to appropriately consider null events. Ultimately, the radar signatures should be considered as another piece of evidence—another confidence builder pointing either toward or away from potential mesovortex and tornado development—that can help a forecaster make the best possible decision when it comes to issuing a severe thunderstorm or tornado warning. It is essential to combine information provided by these radar signatures with conceptual models, environmental information, satellite data, storm spotter reports, and other radar signatures, such as those within the mesovortex warning system when issuing warnings.

Additionally, inherent limitations with *Storm Data*, radar data, and this study's relatively small sample size should also be considered when applying these results. Radar update time may also limit the ability to adequately observe some of these radar signatures, especially at mid- and upper levels where update times are frequently greater than 5 min. To illustrate this idea, we plotted rapid-update KOUN data for every volume scan and every third volume scan (e.g., removed two out of three volume scans to approximate update times provided by current WSR-88D radars) for a mesovortex that produced an EF0 tornado to show midlevel K_{DP} core evolution (Fig. 14). In this case, the maximum value of K_{DP} occurred in between the slower scans and would have made the K_{DP} core appear to be weaker than it actually was. This underestimate could have implications for accurately anticipating mesovortex intensity. In

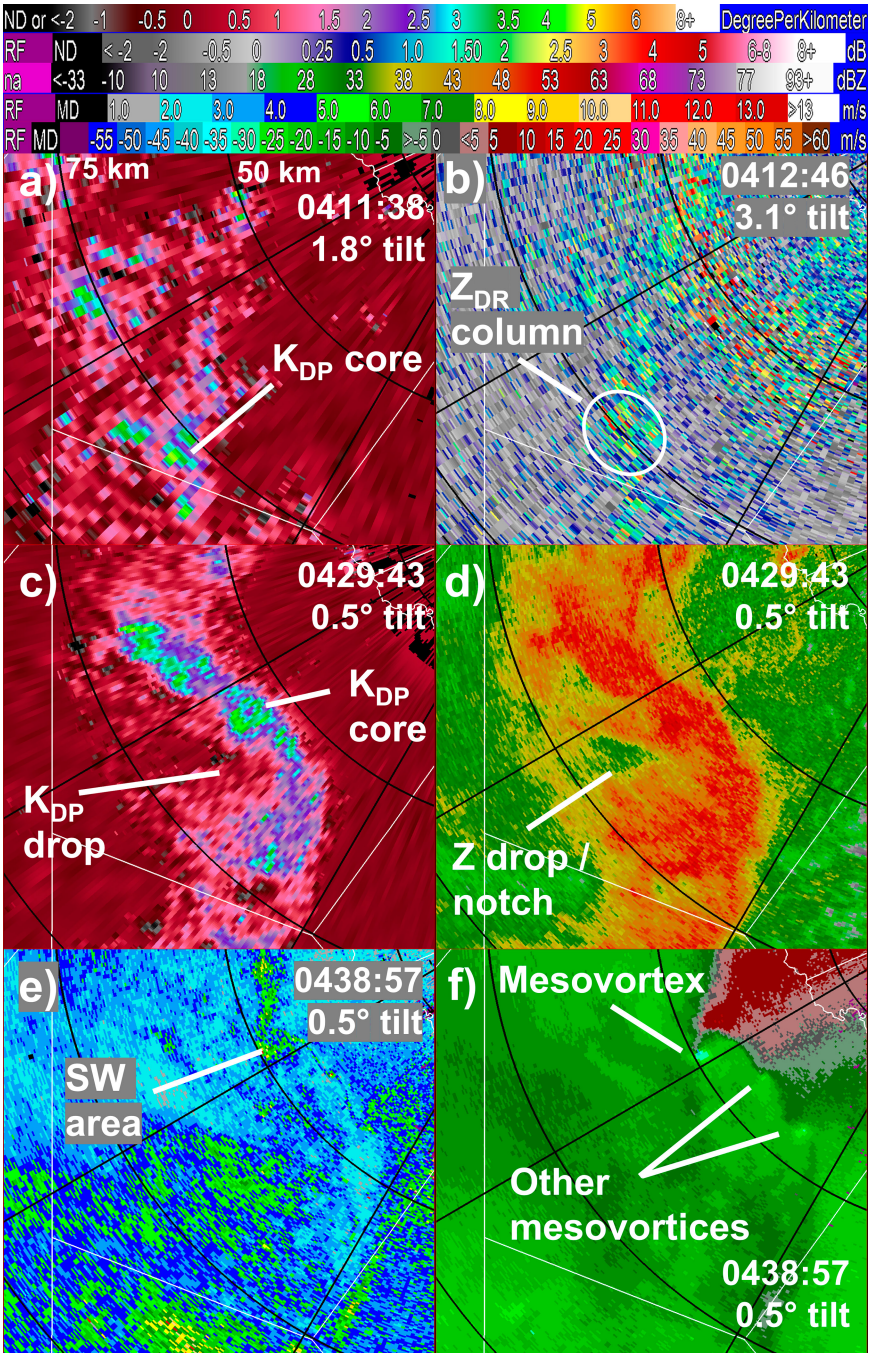

FIG. 13. Example progression of analyzed radar signatures on 20 Feb 2017 in south Texas for (a) midlevel K_{DP} core, (b) Z_{DR} column, (c) K_{DP} drop and low-level K_{DP} core, (d) associated reflectivity (Z) drop/rear-inflow notch, (e) area of enhanced low-level spectrum width (SW area), and (f) mesovortices depicted in ground-relative 0.5° radial velocity. Labeled radar signatures in (a)–(e) are associated with the mesovortex labeled "Mesovortex" in (f). Black curves are range rings every 25 km and are annotated in (a). Color bars for K_{DP}, Z_{DR}, Z, SW, and velocity, respectively, are at the top. North is toward the top of each image.

this example, the maximum midlevel K_{DP} core magnitude of just under 4.5° km^{-1} depicted by the traditional-update data falls just above the median for nontornadic mesovortices, while the maximum magnitude of 5.25° km^{-1} depicted by the rapid-update data falls just under the median for tornadic mesovortices (Figs. 4a and 14). Despite the limitations outlined here, we believe incorporating dual-pol radar signatures into QLCS mesovortex conceptual models and as new confidence builders

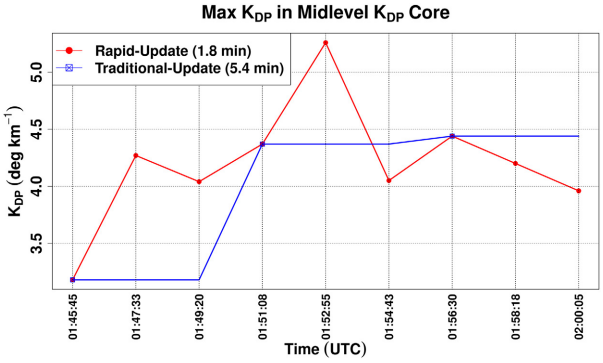

FIG. 14. Comparison of midlevel K_{DP} core maximum value evolution depicted by rapid-update (1.8-min volumes; red line) and traditional-update (5.4-min volumes; blue line) KOUN data associated with a tornadic mesovortex on 11 Oct 2021 in central Oklahoma.

within the mesovortex warning system could aid in warning decision-making by increasing confidence in potential mesovortex development and intensity.

Acknowledgments. C. M. K. thanks God for providing the opportunity and talented research team to accomplish this research. C. M. K. also thanks Emma Kuster and Jami Boettcher for their support and encouragement throughout the research process. The authors thank Todd Lindley, Mark Fox, Richard Smith, and David Andra of NWS Norman for support in the research process; Mike Coniglio, Max Ungar, John Gagan, Justin Gibbs, Tyler Pardun, Jeff Snyder, Jacob Carlin, and Leanne Blind-Doskocil for many helpful conversations regarding QLCSs; Eddie Forren for KOUN data processing; Danny Wasielewski, Chad Smith, Felicia Woolard, Allen Zahrai, Rafael Mendoza, and Micheal Shattuck for KOUN data collection support; Tanya Riley, Tracy Reinke, Jamie Foucher, Mandi Campbell, and Colleen Hickman for help with administrative logistics; Jeff Brogden and Robert Toomey for radar-analysis software support; Steve Fletcher, Zach Tomek, and everyone at NSSL IT for help with computer software/hardware issues; Daphne LaDue and Alex Marmo for the support and help during the 2019 National Weather Center Research Experiences for Undergraduates program; Jacob Carlin, Mike Coniglio, Anthony Lyza, and Matt Bunkers for helpful reviews of the paper; and four anonymous reviewers for helping improve the quality of this paper. Partial funding for C. M. K. and funding for T. J. S. was provided by NOAA/Office of Oceanic and Atmospheric Research under NOAA-University of Oklahoma Cooperative Agreement NA21OAR4320204, U.S. Department of Commerce. A portion of the material is based upon work supported by the National Science Foundation under Grant AGS-1560419.

Data availability statement. All WSR-88D data are available for download from the National Centers for Environmental Information's Radar Archive (https://www.ncdc.noaa.gov/nexradinv/). All KOUN radar data used in this study are available through the National Severe Storms Laboratory at https://data.nssl.noaa.gov/thredds/catalog/customConfig/RRDD/KOUN.html. RAP data used in the environmental analysis can be found at https://www.ncei.noaa.gov/thredds/catalog/model/rucrap.html.

REFERENCES

Anderson-Frey, A. K., and H. Brooks, 2021: Compared to what? Establishing environmental baselines for tornado warning skill. *Bull. Amer. Meteor. Soc.*, **102**, E738–E747, https://doi.org/10.1175/BAMS-D-19-0310.1.

Andra, D. L., Jr., E. M. Quoetone, and W. F. Bunting, 2002: Warning decision making: The relative roles of conceptual models, technology, strategy, and forecaster expertise on 3 May 1999. *Wea. Forecasting*, **17**, 559–566, https://doi.org/10.1175/1520-0434(2002)017<0559:WDMTRR>2.0.CO;2.

Ashley, W. S., A. M. Haberlie, and J. Strohm, 2019: A climatology of quasi-linear convective systems and their hazards in the United States. *Wea. Forecasting*, **34**, 1605–1631, https://doi.org/10.1175/WAF-D-19-0014.1.

Atkins, N. T., and M. St. Laurent, 2009: Bow echo mesovortices. Part II: Their genesis. *Mon. Wea. Rev.*, **137**, 1514–1532, https://doi.org/10.1175/2008MWR2650.1.

——, J. M. Arnott, R. W. Przybylinski, R. A. Wolf, and B. D. Ketcham, 2004: Vortex structure and evolution within bow echoes. Part I: Single-Doppler and damage analysis of the 29 June 1998 derecho. *Mon. Wea. Rev.*, **132**, 2224–2242, https://doi.org/10.1175/1520-0493(2004)132<2224:VSAEWB>2.0.CO;2.

Boyer, C. H., and J. M. L. Dahl, 2020: The mechanisms responsible for large near-surface vertical vorticity within simulated supercells and quasi-linear storms. *Mon. Wea. Rev.*, **148**, 4281–4297, https://doi.org/10.1175/MWR-D-20-0082.1.

Brotzge, J. A., S. E. Nelson, R. L. Thompson, and B. T. Smith, 2013: Tornado probability of detection and lead time as a function of convective mode and environmental parameters. *Wea. Forecasting*, **28**, 1261–1276, https://doi.org/10.1175/WAF-D-12-00119.1.

Chrisman, J. N., 2013: Dynamic scanning. NEXRAD Now, 27 pp., https://www.roc.noaa.gov/wsr88d/PublicDocs/NewTechnology/MESO-SAILS_Description_Briefing_Jan_2014.pdf.

Conrad, D. M., and K. R. Knupp, 2019: Doppler radar observations of horizontal shearing instability in quasi-linear convective systems. *Mon. Wea. Rev.*, **147**, 1297–1318, https://doi.org/10.1175/MWR-D-18-0257.1.

Davis, J. M., and M. D. Parker, 2014: Radar climatology of tornadic and nontornadic vortices in high-shear, low-CAPE environments in the mid-Atlantic and southeastern United States. *Wea. Forecasting*, **29**, 828–853, https://doi.org/10.1175/WAF-D-13-00127.1.

Edwards, R., J. G. LaDue, J. T. Ferree, K. Scharfenberg, C. Maier, and W. L. Coulbourne, 2013: Tornado intensity estimation: Past, present, and future. *Bull. Amer. Meteor. Soc.*, **94**, 641–653, https://doi.org/10.1175/BAMS-D-11-00006.1.

——, H. E. Brooks, and H. Cohn, 2021: Changes in tornado climatology accompanying the enhanced Fujita scale. *J. Appl. Meteor. Climatol.*, **60**, 1465–1482, https://doi.org/10.1175/JAMC-D-21-0058.1.

Fischer, J., and J. M. L. Dahl, 2022: Transition of near-ground vorticity dynamics during tornadogenesis. *J. Atmos. Sci.*, **79**, 467–483, https://doi.org/10.1175/JAS-D-21-0181.1.

Flournoy, M. D., and M. C. Coniglio, 2019: Origins of vorticity in a simulated tornadic mesovortex observed during PECAN on 6 July 2015. *Mon. Wea. Rev.*, **147**, 107–134, https://doi.org/10.1175/MWR-D-18-0221.1.

French, M. M., and D. M. Kingfield, 2021: Tornado formation and intensity prediction using polarimetric radar estimates of updraft area. *Wea. Forecasting*, **36**, 2211–2231, https://doi.org/10.1175/WAF-D-21-0087.1.

Frugis, B. J., 2020: The use of collapsing specific differential phase columns to predict significant severe thunderstorm wind damage across the northeastern United States. Eastern Region Tech. Attachment 2020-04, 16 pp., https://www.weather.gov/media/erh/ta/ta2020-04.pdf.

Fujita, T. T., 1981: Tornadoes and downbursts in the context of generalized planetary scales. *J. Atmos. Sci.*, **38**, 1511–1534, https://doi.org/10.1175/1520-0469(1981)038<1511:TADITC>2.0.CO;2.

Giangrande, S. E., J. M. Krause, and A. V. Ryzhkov, 2008: Automatic designation of the melting layer with a polarimetric prototype of the WSR-88D radar. *J. Appl. Meteor. Climatol.*, **47**, 1354–1364, https://doi.org/10.1175/2007JAMC1634.1.

Gibbs, J. G., 2021: Evaluating precursor signals for QLCS tornado and higher impact straight- line wind events. *J. Oper. Meteor.*, **9**, 62–75, https://doi.org/10.15191/nwajom.2021.0905.

——, and B. R. Bowers, 2019: Techniques and thresholds of significance for using WSR-88D velocity data to anticipate significant tornadoes. *J. Oper. Meteor.*, **7**, 117–137, https://doi.org/10.15191/nwajom.2019.0709.

Goodnight, J. S., D. A. Chehak, and R. J. Trapp, 2022: Quantification of QLCS tornadogenesis, associated characteristics, and environments across a large sample. *Wea. Forecasting*, **37**, 2087–2105, https://doi.org/10.1175/WAF-D-22-0016.1.

Healey, D. J., and M. S. Van Den Broeke, 2023: Comparing polarimetric signatures of proximate pretornadic and nontornadic supercells in similar environments. *Wea. Forecasting*, **38**, 2011–2027, https://doi.org/10.1175/WAF-D-23-0013.1.

Hubbert, J., V. N. Bringi, L. D. Carey, and S. Bolen, 1998: CSU-CHILL polarimetric radar measurements from a severe hail storm in eastern Colorado. *J. Appl. Meteor.*, **37**, 749–775, https://doi.org/10.1175/1520-0450(1998)037<0749:CCPRMF>2.0.CO;2.

Istok, M. J., and R. J. Doviak, 1986: Analysis of the relation between Doppler spectrum width and thunderstorm turbulence. *J. Atmos. Sci.*, **43**, 2199–2214, https://doi.org/10.1175/1520-0469(1986)043<2199:AOTRBD>2.0.CO;2.

James, R. P., and P. M. Markowski, 2010: A numerical investigation of the effects of dry air aloft on deep convection. *Mon. Wea. Rev.*, **138**, 140–161, https://doi.org/10.1175/2009MWR3018.1.

Kumjian, M. R., 2013: Principles and applications of dual-polarization weather radar. Part I: Description of the polarimetric radar variables. *J. Oper. Meteor.*, **1**, 226–242, https://doi.org/10.15191/nwajom.2013.0119.

——, and A. V. Ryzhkov, 2008: Rapid-scan observations of a bow echo storm with a dual-polarization WSR-88D. *24th Conf. on Severe Local Storms*, Savannah, GA, Amer. Meteor. Soc., P4.12, https://ams.confex.com/ams/pdfpapers/141915.pdf.

——, A. P. Khain, N. Benmoshe, E. Ilotoviz, A. V. Ryzhkov, and V. T. J. Phillips, 2014: The anatomy and physics of Z_{DR} columns: Investigating a polarimetric radar signature with a spectral bin microphysical model. *J. Appl. Meteor. Climatol.*, **53**, 1820–1843, https://doi.org/10.1175/JAMC-D-13-0354.1.

——, Z. J. Lebo, and A. M. Ward, 2019: Storms producing large accumulations of small hail. *J. Appl. Meteor. Climatol.*, **58**, 341–364, https://doi.org/10.1175/JAMC-D-18-0073.1.

Kuster, C. M., B. R. Bowers, J. T. Carlin, T. J. Schuur, J. W. Brogden, R. Toomey, and A. Dean, 2021: Using K_{DP} cores as a downburst precursor signature. *Wea. Forecasting*, **36**, 1183–1198, https://doi.org/10.1175/WAF-D-21-0005.1.

Loeffler, S. D., 2017: Dual-polarization signatures in nonsupercell tornadic storms. M.S. thesis, Dept. of Meteorology and Atmospheric Science, The Pennsylvania State University, 44 pp., https://etda.libraries.psu.edu/catalog/14344swl5295.

Marion, G. R., and R. J. Trapp, 2021: Controls of quasi-linear convective system tornado intensity. *J. Atmos. Sci.*, **78**, 1189–1205, https://doi.org/10.1175/JAS-D-20-0164.1.

McDonald, J. M., and C. C. Weiss, 2021: Cold-pool characteristics of tornadic quasi-linear convective systems and other convective modes during VORTEX-SE. *Mon. Wea. Rev.*, **149**, 821–840, https://doi.org/10.1175/MWR-D-20-0226.1.

NWS, 2023: QLCS tornado training. Accessed 24 April 2023, https://www.weather.gov/sgf/qlcs_tornado_training.

Pardun, T. J., 2023: An investigation between tornadic and nontornadic QLCS mesovortices using operational and experimental MRMS products. M.S. thesis, School of Meteorology, University of Oklahoma, 97 pp., https://shareok.org/handle/11244/338758.

Przybylinski, R. W., 1995: The bow echo: Observations, numerical simulations and severe weather detection methods. *Wea. Forecasting*, **10**, 203–218, https://doi.org/10.1175/1520-0434(1995)010<0203:TBEONS>2.0.CO;2.

Sachidananda, M., and D. S. Zrnić, 1987: Rain rate estimates from differential polarization measurements. *J. Atmos. Oceanic Technol.*, **4**, 588–598, https://doi.org/10.1175/1520-0426(1987)004<0588:RREFDP>2.0.CO;2.

Schaumann, J. S., and R. W. Przybylinski, 2012: Operational application of 0–3 km bulk shear vectors in assessing quasi-linear convective system mesovortex and tornado potential. *26th Conf. on Severe Local Storms*, Nashville, TN, Amer. Meteor. Soc., 142 pp., https://ams.confex.com/ams/26SLS/webprogram/Paper212008.html.

Sessa, M. F., and R. J. Trapp, 2020: Observed relationship between tornado intensity and pretornadic mesocyclone characteristics. *Wea. Forecasting*, **35**, 1243–1261, https://doi.org/10.1175/WAF-D-19-0099.1.

Sherburn, K. D., and M. D. Parker, 2014: Climatology and ingredients of significant severe convection in high-shear, low-CAPE environments. *Wea. Forecasting*, **29**, 854–877, https://doi.org/10.1175/WAF-D-13-00041.1.

Smith, B. T., R. L. Thompson, A. R. Dean, and P. T. Marsh, 2015: Diagnosing the conditional probability of tornado damage rating using environmental and radar attributes. *Wea. Forecasting*, **30**, 914–932, https://doi.org/10.1175/WAF-D-14-00122.1.

Snyder, J. C., A. V. Ryzhkov, M. R. Kumjian, A. P. Khain, and J. C. Picca, 2015: A Z_{DR} column detection algorithm to examine convective storm updrafts. *Wea. Forecasting*, **30**, 1819–1844, https://doi.org/10.1175/WAF-D-15-0068.1.

Spoden, P. J., R. A. Wolf, and L. R. Lemon, 2012: Operational uses of spectrum width. *Electron. J. Severe Storms Meteor.*, **7**, 1–28, https://ejssm.org/archives/2012/vol-7-2-2012/.

Thompson, R. L., B. T. Smith, J. S. Grams, A. R. Dean, and C. Broyles, 2012: Convective modes for significant severe thunderstorms in the contiguous United States. Part II: Supercell and QLCS tornado environments. *Wea. Forecasting*, **27**, 1136–1154, https://doi.org/10.1175/WAF-D-11-00116.1.

Trapp, R. J., D. M. Wheatley, N. T. Atkins, R. W. Przybylinski, and R. Wolf, 2006: Buyer beware: Some words of caution on the use of severe wind reports in postevent assessment and research. *Wea. Forecasting*, **21**, 408–415, https://doi.org/10.1175/WAF925.1.

Tuttle, J. D., V. N. Bringi, H. D. Orville, and F. J. Kopp, 1989: Multiparameter radar study of a microburst: Comparison with model results. *J. Atmos. Sci.*, **46**, 601–620, https://doi.org/10.1175/1520-0469(1989)046<0601:MRSOAM>2.0.CO;2.

Ungar, M. D., and M. C. Coniglio, 2023: Using radiosonde observations to assess the "three ingredients method" to forecast QLCS mesovortices. *Wea. Forecasting*, **38**, 2441–2460, https://doi.org/10.1175/WAF-D-22-0176.1.

Van Den Broeke, M. S., 2020: A preliminary polarimetric radar comparison of pretornadic and nontornadic supercell storms. *Mon. Wea. Rev.*, **148**, 1567–1584, https://doi.org/10.1175/MWR-D-19-0296.1.

WDTD, 2011: Dual-polarization radar principles and system operations. Accessed 15 December 2023, https://training.weather.gov/wdtd/courses/dualpol/documents/DualPolRadarPrinciples.pdf.

——, 2020: WOC severe QLCS. Accessed 15 October 2023, https://training.weather.gov/wdtd/courses/woc/severe/storm-structures-hazards/storm-modes/qlcs/presentation_html5.html.

Weisman, M. L., and R. J. Trapp, 2003: Low-level mesovortices within squall lines and bow echoes. Part I: Overview and dependence on environmental shear. *Mon. Wea. Rev.*, **131**, 2779–2803, https://doi.org/10.1175/1520-0493(2003)131<2779:LMWSLA>2.0.CO;2.

Wheatley, D. M., and R. J. Trapp, 2008: The effect of mesoscale heterogeneity on the genesis and structure of mesovortices within quasi-linear convective systems. *Mon. Wea. Rev.*, **136**, 4220–4241, https://doi.org/10.1175/2008MWR2294.1.

Wilson, M. B., and M. S. Van Den Broeke, 2021: Using the Supercell Polarimetric Observation Research Kit (SPORK) to examine a large sample of pretornadic and nontornadic supercells. *Electron J. Severe Storms Meteor.*, **17** (2), https://doi.org/10.55599/ejssm.v17i2.85.

Witt, A., M. D. Eilts, G. J. Stumpf, J. T. Johnson, E. D. Mitchell, and K. W. Thomas, 1998: An enhanced hail detection algorithm for the WSR-88D. *Wea. Forecasting*, **13**, 286–303, https://doi.org/10.1175/1520-0434(1998)013<0286:AEHDAF>2.0.CO;2.

Zrnić, D. S., N. Balakrishnan, C. L. Ziegler, V. N. Bringi, K. Aydin, and T. Matejka, 1993: Polarimetric signatures in the stratiform region of a mesoscale convective system. *J. Appl. Meteor.*, **32**, 678–693, https://doi.org/10.1175/1520-0450(1993)032<0678:PSITSR>2.0.CO;2.